TITLE:

Low dose exposure diagnosis with a transXend detector aiming for iodine-marked cancer detection

AUTHOR(S):

Kanno, Ikuo; Shimazaki, Hironobu; Imamura, Ryo; Yamashita, Yoshiki; Shima, Kazunari; Ohtaka, Masahiko; Hashimoto, Makoto; Ara, Kuniaki; Onabe, Hideaki

CITATION:

Kanno, Ikuo ...[et al]. Low dose exposure diagnosis with a transXend detector aiming for iodine-marked cancer detection. Journal of Nuclear Science and Technology 2012, 49(9): 937-946

ISSUE DATE:

2012-08-21

URL:

http://hdl.handle.net/2433/178661

RIGHT:

This is a preprint of an article whose final and definitive form has been published in the Journal of Nuclear Science and Technology © 2012 Taylor & Francis; Journal of Nuclear Science and Technology is available online at: www.tandfonline.com with the open URL of your article; この論文は出版社版でありません。引用の際には出版社版をご確認ご利用ください。; This is not the published version. Please cite only the published version.

京都大学学術情報リポジトリ
KURENAI 紅
Kyoto University Research Information Repository

京都大学 KYOTO UNIVERSITY
A Self-archived copy in
Kyoto University Research Information Repository
https://repository.kulib.kyoto-u.ac.jp
京都大学学術情報リポジトリ KURENAI 紅 Kyoto University Research Information Repository

ARTICLE

Low Dose Exposure Diagnosis with a transXend Detector Aiming for Iodine-marked Cancer Detection

Ikuo Kanno[a,*], Hironobu Shimazaki[a], Ryo Imamura[a], Yoshiki Yamashita[a], Kazunari Shima[a], Masahiko Ohtaka[b], Makoto Hashimoto[b], Kuniaki Ara[b] and Hideaki Onabe[c]

[a] *Graduate School of Engineering, Kyoto University, Sakyo, Kyoto 606-8501, Japan*

[b] *O-arai Research and Development Institute, Japan Atomic Energy Agency, Narita, O-arai, Ibaraki 311-1393, Japan*

[c] *Raytech Corporation, Yoto, Utsunomiya 321-0904, Japan*

(*Received*)

The energy resolved computed tomography (CT), that had advantage over conventional CT (twofold higher CT value for iodine contrast agent and being free from beam hardening effect), was shown practical by employing the transXend detector: it measured X-rays as electric current and gave energy distribution of incident X-rays after analysis. This paper shows a new application of the transXend detector for estimating the thicknesses of acrylic, iodine and aluminum in a phantom. For this purpose, the responses of the segment detectors in the transXend detector are changed intentionally with inserting filters. With previously obtained two-dimensional maps for acrylic-iodine, and acrylic-aluminum thicknesses, which are shown by the ratios of electric currents measured by the segment detectors, the thickness of materials on the path of the X-rays are obtained by a transmission measurement.

KEYWORDS: X-ray, transmission measurement, contrast agent, computed tomography, dose exposure, energy resolved CT

[*]Corresponding author, E-mail: kanno@nucleng.kyoto-u.ac.jp

京都大学 KYOTO UNIVERSITY
A Self-archived copy in
Kyoto University Research Information Repository
https://repository.kulib.kyoto-u.ac.jp
京都大学学術情報リポジトリ KURENAI 紅 Kyoto University Research Information Repository

1. Introduction

X-ray computed tomography (CT) is a powerful tool for finding tumors, including cancers. To observe cancers more clearly, contrast agent such as iodine is injected into a blood vessel. There are many more blood vessels in cancer tissue than in normal tissue; as a result, the iodine concentration is higher in cancer tissue than in normal tissue. This method of examination is called contrast-enhanced CT. The estimated iodine thickness in 1 cm thick cancer in the direction of X-ray transmission ranges from 1 to 60 μm[1,2].

Iodine has X-ray absorption K-edge at the energy of 33.2 keV. The X-rays with their energy higher than 33.2 keV are absorbed by iodine strongly. The numbers of X-rays passing through cancer tissue with iodine and through normal tissue differ much. As a result, the CT values of cancer tissue and normal tissue have different values.

Contrast-enhanced CT has two major problems: high dose exposure and side effects of the iodine contrast agent[3]. Another problem is a beam hardening effect: X-ray absorption by iodine is difficult to detect with high X-ray tube voltage and a large subject[4].

We have been working on solving these problems by measuring the energy of X-rays: conventional X-ray CT measures X-rays as electric current and does not use energy information of X-rays. The use of energy information of X-rays gives following advantages: (1) X-ray absorption by iodine is observed in the same way despite of the X-ray tube voltage and of the thickness of the subject (beam hardening effect free)[2], (2) CT value of iodine is nearly twofold higher than the one obtained by current measurement CT[5], (3) dose exposure is reduced to 1/2 to 1/3 when an X-ray filter, such as a lanthanum filter, is applied at the exit of X-ray tube[1].

Measuring energy of X-rays, however, takes long time due to the limitation of time duration of electric carriers to reach positive and negative electrodes in any type of X-ray detectors. On the other hand, CT measurements should be performed in a very short time, in the order of seconds. X-ray detectors with high counting rate are under development

京都大学 KYOTO UNIVERSITY
A Self-archived copy in
Kyoto University Research Information Repository
https://repository.kulib.kyoto-u.ac.jp
京都大学学術情報リポジトリ KURENAI 紅 Kyoto University Research Information Repository

intensively, such as Medipix-2: it can measure one million X-rays in a second, however, the energy of X-rays should be less than 30 keV, while the maximum energy of X-rays used in diagnosis ranges 80-150 keV[6].

As an X-ray detector to give energy information for CT measurements, we invented a novel system, called the transXend detector, which measures X-rays as electric current, and after analysis, provides the energy distribution of X-rays[7]. The transXend detector consists of several segment detectors aligned along the direction of the X-ray incidence, as shown in Fig. 1. Each segment detector measures X-rays as electric current. Segment detectors in the forward absorb low energy X-rays, and some portion of high energy X-rays. The rearward segment detectors do not have low energy X-rays much, but higher energy X-rays. According to the materials and the position of segment detectors, the responses of the segment detectors to X-rays change. With previously obtained response functions for segment detectors, the energy distribution of incident X-rays is obtained by unfolding a matrix equation. The substrate of segment detectors can be semiconductors, scintillators, and any other materials that have been employed for radiation detectors.

The response functions for segment detectors are desired not to be similar: otherwise, obtained X-ray energy distribution strongly depends on an initial guess in the unfolding process. To change response functions of segment detectors, scintillators with various atomic numbers and densities were employed. Comparing to the transXend detector with various scintillator segment detectors to the one with the same scintillator segment detectors, X-ray energy distribution which did not depend on the initial guess was obtained by various scintillator transXend detector with even less amount of the product of X-ray tube current and time, *i.e.*, mAs[8].

The energy resolved CT has advantages over conventional current measurement CT, however, it requires X-ray exposures through 360 degrees around a subject, the same as in the conventional CT measurements: the conventional CT takes nearly 1,000 transmission images

京都大学 KYOTO UNIVERSITY
A Self-archived copy in
Kyoto University Research Information Repository
https://repository.kulib.kyoto-u.ac.jp
京都大学学術情報リポジトリ KURENAI 紅 Kyoto University Research Information Repository

in 360 degree roration[9]. In this paper, we propose a novel method for estimating thicknesses of known materials in a subject with one X-ray transmission measurement, with using two-dimensional maps made of the ratio of electric currents measured by the segment detectors of the transXend detector. The two-dimensional maps are equivalent to the response functions employed in the unfolding process in the analysis of transXend detector measurements.

2. Two-dimensional Map using the Outputs of the transXend Detector

For the transXend detector with three segment detectors made of Si(Li), simulation study was performed. The thickness of Si(Li) detector was 1 mm. With the tube voltage 120 kV, X-rays were emitted through 2 mm thick aluminum filter and 20 cm thick air before entering a phantom, which consisted of acrylic (a substitute of soft tissue) layer and iodine layer (a substitute of cancer tissue marked with iodine) with various thicknesses. X-ray energy spectrum was calculated according to Ref. [10].

The energy spectrum of X-rays before entering the first segment detector, $Y_1(E)$, is described as,

$$Y_1(E) = Y_0(E) \cdot \exp\{-(\mu_A(E)/\rho_A \cdot \rho_A t_A + \mu_I(E)/\rho_I \cdot \rho_I t_I)\}. \quad (1)$$

Here, $Y_0(E)$ is the number of X-rays with energy E before entering into acrylic and iodine layers, $\mu_A(E)/\rho_A$, $\mu_I(E)/\rho_I$, ρ_A, ρ_I, t_A, and t_I are the mass attenuation coefficients, densities and thicknesses of acrylic and iodine, respectively. The electric current measured by the first segment detector is written as,

$$I_1 \propto \int E \cdot Y_1(E) \cdot \{1 - \exp(-\mu_{en}(E)/\rho_S \cdot \rho_S t_S)\} dE \quad . \quad (2)$$

Here, $\mu_{en}(E)/\rho_S$, ρ_S and t_S are the mass-energy absorption coefficient, density and thickness of detector substrate, *i.e.*, silicon. The electric currents measured by the second and third segment detectors can be calculated in the same way but the incident number of X-rays is decreased by the absorption of forward segment detectors. With defining the currents

京都大学 KYOTO UNIVERSITY
A Self-archived copy in
Kyoto University Research Information Repository
https://repository.kulib.kyoto-u.ac.jp
京都大学学術情報リポジトリ KURENAI 紅 Kyoto University Research Information Repository

measured by the first, second and third segment detectors as I_1, I_2 and I_3, the current ratios I_2/I_1 and I_3/I_1 are calculated.

Similar calculations are carried out for the transXend detector with a 300 μm thick Sn filter in front of the third segment detector. Simulation results are shown in Fig. 2 for the cases with and without the Sn filter. Without the Sn filter, the increments of acrylic and iodine thicknesses in the two-dimensional map would fall on the same line. The current ratios measured by the transXend detector with the Sn filter, however, showed different directions for acrylic and iodine increments. This two-dimensional map for acrylic-iodine thickness means that a simple X-ray transmission measurement is enough to give information regarding tissues marked with iodine contrast agent.

3. Experiments

3.1. Two Materials Identification

Experimental setup is shown in Fig. 3. Employed transXend detector consists of three Si(Li) segment detectors. The dimensions of Si(Li) are 10×10×1 mm^3. Bias voltage is not applied to Si(Li) detectors during operation: the mean free paths of electrons and holes in Si is greater than 1 mm[11]. The Si(Li) transXend detector was operated at room temperature.

The transXend detector has two configurations: with and without a Sn filter (58 μm in thickness) in front of the third Si(Li) segment detector. The X-ray tube is TRIX-150S (Toreck Co. Ltd., Japan). The tube voltage and current are 120 kV and 2.4 mA, respectively. Collimators are placed at the exit of the X-ray tube and the entrance of the transXend detector.

The X-ray tube voltage, the thicknesses of acrylic phantom and the Sn filter were chosen with considering the maximum current of the X-ray tube: for medical diagnosis, X-ray tubes with 200-300 mA of tube current are employed to inspect a human body with the thickness of nearly 20 cm. For current measurement of X-rays (a number of X-rays should come into an X-ray detector simultaneously) with using a low current X-ray tube, a phantom

京都大学 KYOTO UNIVERSITY
A Self-archived copy in
Kyoto University Research Information Repository
https://repository.kulib.kyoto-u.ac.jp
京都大学学術情報リポジトリ KURENAI 紅 Kyoto University Research Information Repository

much thinner than the human body must be employed.

X-rays after passing a phantom, which consists of acrylic slabs and an iodine region, are measured by three segment detectors, as electric currents, I_1, I_2, and I_3. The thickness of acrylic is changed from 7 to 77 mm with the interval of 10 mm. Also, four iodine regions are prepared in an acrylic slab. The iodine thicknesses are adjusted to be 15 to 60 μm with the interval of 15 μm by thinning iodine tincture with water. With taking the current ratios I_2/I_1 and I_3/I_1 as *x*- and *y*-axes, measured results by the transXend detector with the Sn filter are plotted as shown in Fig. 4. With inserting the Sn filter, the directions of acrylic and iodine increments change apart each other, and result in two-dimensional map, as predicted by the simulation study.

Because we have only one set of the transXend detector, we performed scanning measurements of a phantom. The phantom is a cylindrical acrylic with the diameter of 30 mm and has a 5 mm diameter hole for thinned iodine tincture 5 mm apart from the phantom center, as shown in Fig. 5 (a). The thickness of iodine is 15 μm in 5 mm distance of X-ray transmission. The scanning step is 0.4 mm. Obtained current ratios are put into the two-dimensional map shown in Fig. 4 and the acrylic and iodine thicknesses are estimated. The thickness distributions for acrylic and iodine are shown in Fig. 6.

3.2. Three Materials Identification

For taking into account of bone in the human body, an aluminum rod is inserted in an acrylic phantom as a substitute for bone. The schematic drawing of the acrylic phantom is shown in Fig. 5 (b). The diameter of the aluminum rod is 2 mm. The centers of the iodine region and the aluminum rod are 7.5 mm from the center of the phantom in the opposite directions. The thickness of iodine is the same as described in section *3.1*.

Employed transXend detector is the same one used in section *3.1*., but the fourth Si(Li) segment detector is added with Gd filter in front of it. The thickness of the Gd filter is

京都大学 KYOTO UNIVERSITY
A Self-archived copy in
Kyoto University Research Information Repository
https://repository.kulib.kyoto-u.ac.jp
京都大学学術情報リポジトリ KURENAI 紅 Kyoto University Research Information Repository

75 μm. In this measurement of estimating acrylic, iodine and aluminum thicknesses, acrylic-iodine and acrylic-aluminum maps are necessary. For the acrylic-iodine map, the same procedure described in the previous section is repeated. For the acrylic-aluminum map, electric currents induced by X-rays after passing acrylic with the thickness of 6 to 66 mm with 10 mm interval, and aluminum with the thickness of 1 to 4 mm with 1 mm interval are measured. Obtained two-dimensional maps are shown in Fig. 7 (a) and (b) for acrylic-iodine and acrylic-aluminum, respectively. Figure 7 (a) is the same with Fig. 4, but drawn for small values of I_2/I_1 and I_3/I_1. In Fig. 7 (b), I_3/I_1 and I_4/I_3 are employed for x and y-axes: the current value of I_4 is very small comparing to I_1.

As with the same way, the acrylic phantom with iodine and aluminum is scanned with a step of 0.4 mm. Obtained current ratios of scanned results are plotted in Fig. 7 (a) and (b) by solid lines. The results are analyzed in the same way as in the previous section.

4. Results and Discussions

4.1. Thickness Distributions of Acrylic and Iodine

In Fig. 6, the expected thickness distributions of acrylic and iodine are shown by dashed lines. Because the collimator in front of the transXend detector has 2 mm width, the theoretical thickness at the position x, $t_k(x)$, is the averaged ones from $x-1$ mm to $x+1$mm. Here, k means the acrylic or iodine.

In the case of the thickness distribution of acrylic, the thicknesses close to $x=\pm 15$ mm agree very nicely to the theoretical acrylic thickness. The thicknesses of acrylic close to the center slightly deviate from the theoretical ones.

The iodine thicknesses in the iodine region show excellent agreement with the theoretical ones. The iodine thicknesses at both ends of the iodine region, however, are overestimated to some extent. These overestimated iodine thicknesses result in the underestimation of corresponding acrylic thicknesses. The iodine thicknesses at positive x

京都大学 KYOTO UNIVERSITY
A Self-archived copy in
Kyoto University Research Information Repository
https://repository.kulib.kyoto-u.ac.jp
京都大学学術情報リポジトリ KURENAI 紅 Kyoto University Research Information Repository

show positive values, although they should be zero. We suspect that this phenomenon is the result of energy spectrum change of X-rays during experiment: a simple change in X-ray tube current does not give any harm to the measurements, because the change of X-ray numbers emitted in the unit time is canceled with using the current ratios, I_2/I_1 and I_3/I_1. The correction method for X-ray energy spectrum change is the theme of study for practical use of this method.

4.2. Thickness Distributions of Acrylic, Iodine and Aluminum

4.2.1. Effect of Hidden Materials

In Fig. 7 (a) and (b), two-dimensional maps for acrylic-iodine and acrylic-aluminum are plotted as well as the scanned traces by solid lines. Also, measurement results for reference points (see Table 1) are plotted by pluses (+). In Fig. 7 (a), points *a*, *b*, and *c* are on the symbols, and points *d*, *e*, and *f* are on the symbols in Fig. 7 (b).

In Fig. 7 (a), the scanned trace starts from the point at which there is air only and goes to point *a* (with 7 mm thick acrylic). After point *a*, the scan moves to the point with 17 mm thick acrylic and then goes slightly upward to the part with iodine (acrylic thickness between 17 - 27 mm). After passing the iodine region, the scan comes back on the line with no iodine and reaches to the center of acrylic phantom. Although the X-ray passing distance becomes shorter after leaving the center, the scanned points are in a region where the acrylic thicknes is greater than 30 mm as seen at the points close to *f*, where the acrylic thickness is 47 mm. The scan results around here have the effect of X-ray absorption by aluminum but are observed as the results for acrylic because the two-dimensional map of Fig. 7 (a) does not include the X-ray absorption by aluminum.

In Fig. 7 (b), the scanned points pass *d* and go through the point close to *b*. The scan then moves to a point close to *c* and reaches the point where acrylic has 46 mm thickness, close to the point (0.400, 0.250). This is the effect of X-ray absorption by iodine. The scan

京都大学 KYOTO UNIVERSITY
A Self-archived copy in
Kyoto University Research Information Repository
https://repository.kulib.kyoto-u.ac.jp
京都大学学術情報リポジトリ KURENAI 紅 Kyoto University Research Information Repository

comes back to the point between 26-36 mm acrylic thickness when the X-rays pass the center of the acrylic phantom. After leaving the center, X-rays are absorbed by aluminum. At this stage, the scanned data comes close to the square symbol (0.400, 0.248) and reaches a point close to (0.405, 0.250). After passing the center of the aluminum rod, the scan comes back to the part with acrylic only, then to the point with only air.

With neglecting the effects of hidden materials and taking the scanned data as the absorption of X-rays by acrylic and iodine in Fig. 7 (a), and by acrylic and aluminum in Fig. 7 (b), acrylic-iodine and acrylic-aluminum thickness distributions are obtained and shown in Fig. 8 (a) and (b). In Fig. 8 (a), the thickness of acrylic is overestimated at $x = +7.5\,\mathrm{mm}$, where the aluminum rod is in the phantom. In contrast, the iodine thickness distribution has a dip at the same position. The overestimation and underestimation described above are attributed to the aluminum rod, which is hidden in this figure but is seen in Fig. 7 (a). The same phenomena are seen in Fig. 8 (b): The acrylic and aluminum thicknesses are overestimated at $x = -7.5\,\mathrm{mm}$, where the iodine region is in the phantom.

4.2.2. Estimation of Hidden Materials

To estimate X-ray absorption by hidden materials (*i.e.*, aluminum in Fig. 8 (a) and iodine in Fig. 8 (b)), the estimated acrylic, iodine, and aluminum thicknesses of reference points *a* to *f* shown in Table 1 are plotted in Fig. 9 (a) and (b). In Fig. 9 (a), points *a*, *b* and *c* are aligned vertically because the iodine thickness is measured in the vertical axis. At point *d*, the iodine thickness should be zero, but it had a slightly negative value due to the change of X-ray energy spectrum as described in section *4.1*. This X-ray tube is known to have instability of this magnitude. From point *d* to *f*, the aluminum thickness increases 2 mm. With fitting the points *d* to *f* by the least square method, the change in aluminum thickness is shown comparable to an acrylic thickness of 41 mm and an iodine thickness of – 3.5 μm.

Also, the iodine thickness increases 30 μm from point *a* to *c*, in Fig. 9 (b). With

京都大学 KYOTO UNIVERSITY
A Self-archived copy in
Kyoto University Research Information Repository
https://repository.kulib.kyoto-u.ac.jp
京都大学学術情報リポジトリ KURENAI 紅 Kyoto University Research Information Repository

fitting the points *a*, *b* and *c*, the iodine thickness increment results in acrylic with 29 mm thickness, and 0.38 mm aluminum thickness.

We assume that the thicknesses of acrylic and iodine are described as vectors $\vec{\alpha}$ and $\vec{\beta}$, which are independent each other, as shown in Fig. 9 (a). The estimated thickness distributions of acrylic and iodine in Fig. 8 (a) are denoted $P_1(x)\cdot\vec{\alpha}$, and $P_2(x)\cdot\vec{\beta}$, where *x* indicates the phantom position. Similarly, acrylic and aluminum thickness distributions in Fig. 8 (b) are denoted $Q_1(x)\cdot\vec{\alpha}$ and $Q_2(x)\cdot\vec{\gamma}$.

With the estimation of X-ray absorption by hidden materials described above, the effect of aluminum in Fig. 8 (a) is estimated as $\frac{41000}{2000}\cdot\vec{\alpha}-\frac{3.5}{2000}\cdot\vec{\beta}$ and that for iodine in Fig. 8 (b) is, $\frac{29000}{30}\cdot\vec{\alpha}+\frac{380}{30}\cdot\vec{\gamma}$. Here, 41000/2000 and –3.5/2000 mean that the increase of aluminum thickness 2 mm is reflected in the increase in acrylic thickness of 41 mm, and for that of iodine thickness –3.5 μm, respectively. Writing the thickness distributions of acrylic, iodine, and aluminum as $A(x)$, $B(x)$ and $C(x)$, we have following equations,

$$A(x)\cdot\vec{\alpha}+B(x)\cdot\vec{\beta}+\left(\frac{41000}{2000}\cdot\vec{\alpha}-\frac{3.5}{2000}\cdot\vec{\beta}\right)\cdot C(x)=P_1(x)\cdot\vec{\alpha}+P_2(x)\cdot\vec{\beta}\,, \tag{3}$$

$$A(x)\cdot\vec{\alpha}+\left(\frac{29000}{30}\cdot\vec{\alpha}+\frac{380}{30}\cdot\vec{\gamma}\right)\cdot B(x)+C(x)\cdot\vec{\gamma}=Q_1(x)\cdot\vec{\alpha}+Q_2(x)\cdot\vec{\gamma}\,. \tag{4}$$

With these two equations, we have,

$$P_1(x)=A(x)+\frac{41000}{2000}C(x),\quad P_2(x)=B(x)-\frac{3.5}{2000}C(x),$$

$$Q_1(x)=A(x)+\frac{29000}{30}B(x),\quad Q_2(x)=\frac{380}{30}B(x)+C(x)\ . \tag{5}$$

After solving these simultaneous equations, $A(x)$, $B(x)$ and $C(x)$ are obtained as shown in Fig. 10.

京都大学 KYOTO UNIVERSITY
A Self-archived copy in
Kyoto University Research Information Repository
https://repository.kulib.kyoto-u.ac.jp
京都大学学術情報リポジトリ KURENAI 紅 Kyoto University Research Information Repository

4.2.3. Estimated Results

Similar to Fig. 6, theoretical thickness distributions for acrylic, iodine and aluminum are shown by dashed lines in Fig. 10. Here, aluminum thickness 1 mm is normalized to 15 μm thick iodine for easy comparison. The thickness distribution of aluminum shows excellent agreement with the theoretical one at the place where the aluminum rod is in. On the contrary, the iodine thickness distribution in the iodine region is overestimated. This phenomenon is expected from Fig. 7 (a): the scan data exceeds the iodine thickness 15 μm at the point (0.878, 0.40). This overestimation is related to the underestimation of the acrylic thickness distribution at $x = -7.5$ mm. Also, the iodine thickness in the positive positions results in the underestimation of corresponding acrylic thickness. Although we have some deviations from the theoretical thickness distributions, we can find iodine and aluminum in their places.

4.3. Origin of Two Dimensional Map

The photon numbers deposited in a Si(Li) segment detector, $Y(E)$, are calculated for the changes of acrylic and iodine thicknesses with the same conditions of Fig. 2. The calculated results are shown in Figs. 11 and 12 for acrylic and iodine thickness increments for the (a) first, (b) second, (c) third segment detectors, and the (d) third segment detectors with Sn filter in front of it, respectively. Without the Sn filter, the energy spectra of deposited X-rays slightly become harder as the X-rays pass through segment detectors. With the Sn filter, the deposited X-rays change their energy spectra drastically.

The decrease of X-ray numbers as a function of acrylic thickness increment is nearly the same for the cases with and without Sn filter as seen in Fig. 11. On the contrary, the iodine thickness increase with the Sn filter (Fig. 12 (d)) shows less decrement, comparing with the ones without the Sn filter (Fig. 12 (a)-(c)).

京都大学 KYOTO UNIVERSITY
A Self-archived copy in
Kyoto University Research Information Repository
https://repository.kulib.kyoto-u.ac.jp
京都大学学術情報リポジトリ KURENAI 紅 Kyoto University Research Information Repository

The electric current, *I*, is the integral of the product of the number of X-rays, $Y(E)$, and their energy, *E*. Without the Sn filter, the decrements of I_1, I_2 and I_3 are nearly the same as functions of acrylic and iodine thicknesses and result in the symbols in Fig. 2 which are on the same line. In the case of placing the Sn filter in front of the third segment detector, the decrement of I_3 as a function of iodine thickness is smaller than the one as a function of acrylic thickness. These differences make the two-dimensional map for acrylic-iodine thicknesses in Fig. 2.

4.4. Three Dimensional Map

In this paper, two-dimensional maps for acrylic-iodine and acrylic-aluminum are prepared before estimating the thickness distributions of these materials in the phantom. As a result, effects of hidden materials should be taken into account in the analysis. If a three-dimensional map for acrylic, iodine and aluminum can be prepared, thickness distributions of these materials are obtained directly. The number of measurements for obtaining a necessary map, however, increases drastically as $m \times n \times l$, instead of $m \times (n + l)$, where *m*, *n*, and *l* are the numbers of thickness change for acrylic, iodine and aluminum, respectively.

5. Conclusion

The energy resolved computed tomography (CT) has been demonstrated its possibility in reducing the amount of iodine contrast agent, and being free from the beam hardening effect. The transXend detector makes the energy resolved CT a practical diagnosis method.

In this paper, we proposed a novel method of applying the transXend detector for estimating the thicknesses of known materials in a phantom. With the previously obtained two-dimensional maps for the combinations of thicknesses of two materials in the phantom, the thicknesses of materials in the X-ray transmission path are estimated: the two-dimensional

京都大学 KYOTO UNIVERSITY
A Self-archived copy in
Kyoto University Research Information Repository
https://repository.kulib.kyoto-u.ac.jp
京都大学学術情報リポジトリ KURENAI 紅 Kyoto University Research Information Repository

maps correspond to the response functions employed in the unfolding process of the output electric currents of the transXend detector. Although we have over- and under-estimations in the thickness distributions, we can detect the places where we have iodine and aluminum in the acrylic phantom. This method requires only one transmission measurement for detecting iodine-marked tissue and reduces the dose exposure much. With a small number of transmission measurements for different angles to the subject, the shape and the position of cancer tissue can be visualized.

Acknowledgements

The authors are thankful to Prof. K. Watanabe, Nagoya University for discussion. A part of this work was supported by the Suzuken Memorial Foundation.

京都大学 KYOTO UNIVERSITY
A Self-archived copy in
Kyoto University Research Information Repository
https://repository.kulib.kyoto-u.ac.jp
京都大学学術情報リポジトリ KURENAI 紅 Kyoto University Research Information Repository

References

1) I Kanno, S. Maetaki, H. Aoki, S. Nomiya and H. Onabe, "Low exposure X-ray transmission measurements for contrast media detection with filtered X-rays", *J. Nucl. Sci. Technol*., **40**, 457-463 (2003).

2) I. Kanno, A. Uesaka, S. Nomiya and H. Onabe, "Energy measurement of X-rays in computed tomography for detecting contrast media", *J. Nucl. Sci. Technol*., **45**, 15-24 (2008).

3) H. Katayama, K. Yamaguchi, T. Kozuka, T. Takashima, P. Seez, K. Matsuura, "Adverse reactions to ionic and nonionic contrast media. A report from the Japanese committee on the safety of contrast media", *Radiology*, **175**, 621-628 (1990).

4) R. A. Brooks, G. Di Chiro, "Beam hardening in X-ray reconstructive tomography", *Phys. Med. Biol*., **21**, 390-398 (1976).

5) I. Kanno, A. Uesaka, S. Nomiya, H. Onabe, "Comparison of current and energy X-ray measurement methods in contrast media detection", *Nucl. Instrum. Methods in Phys. Res*., **A580**, 534-536 (2007).

6) A. P. H. Butler, N. G. Anderson, R. Tipples, N. Cook, R. Watts, J. Meyer, A. J. Bell, T. R. Melzer, P. H. Butler, "Bio-medical X-ray imaging with spectroscopic pixel detectors", *Nucl. Instrum. Methods in Phys. Res*., **A591**, 141-146 (2008).

7) I. Kanno, R. Imamura, K. Mikami, A.Uesaka, M. Hashimoto, M. Ohtaka, K. Ara, S. Nomiya, H. Onabe, "A current-mode detectorfor unfolding X-ray energy distribution", *J. Nucl. Sci. Technol*., **45**, 1165-1170 (2008).

8) I. Kanno, Y. Minami, R. Imamura, H. Shimazaki, K. Fukuda, M. Ohtaka, M. Hashimoto, K. Ara, H. Onabe, "Advantages of response function change in a transXend detector with various scintillators as substrates of segment detectors", *J. Nucl. Sci. Technol*., **48**, 1377-1384 (2011).

9) S. Ramani, J. A. Fessler, "A splitting-based iterative algorithm for accelerated statistical X-ray CT reconstruction", *IEEE Trans. on Med. Imaging*, **31**, 677-688 (2012).

10) R. Birch, M. Marshall, "Computation of bremsstrahlung X-ray spectra and comparison

京都大学 KYOTO UNIVERSITY
A Self-archived copy in
Kyoto University Research Information Repository
https://repository.kulib.kyoto-u.ac.jp
京都大学学術情報リポジトリ KURENAI 紅 Kyoto University Research Information Repository

with spectra measured with a Ge(Li) detector", *Phys. Med. Biol*., **24**, 505-517 (1979).

11) Y. Naruse, T. Kobayashi, "Multichannel semiconductor detectors for high energy X-ray and electron beams", *Nucl. Instrum. Methods*, **191**, 173-175 (1982).

京都大学 KYOTO UNIVERSITY
A Self-archived copy in
Kyoto University Research Information Repository
https://repository.kulib.kyoto-u.ac.jp
京都大学学術情報リポジトリ KURENAI 紅 Kyoto University Research Information Repository

Figure captions

Table 1　Reference points for the correction of hidden materials in two-dimensional maps.

Figure 1 Schematic drawing of a transXend detector.

Figure 2　Calculated two-dimensional map of I_2/I_1-I_3/I_1 for the cases without and with a Sn filter. The X-ray tube voltage and Sn filter thickness are 120 kV and 300 μm, respectively. The acrylic thickness is indicated in the figure. The iodine thicknesses are 0 μm (dots), 10 μm (squares), 20 μm (diamonds), 30 μm (up triangles) and 40 μm (down triangles), respectively.

Figure 3 Experimental setup. Acrylic slabs, an acrylic with iodine regions in it, and step phantom of aluminum are employed for two-dimensional map measurements. For the scanning measurements, cylindrical phantoms in Fig. 5 are used.

Figure 4 Two-dimensional map for acrylic and iodine thicknesses estimation. Acrylic phantom thickness ranges from 7 to 77 mm with 10 mm intervals. Iodine thickness is shown in the figure.

Figure 5 Schematic drawings of acrylic phantoms for (a) acrylic-iodine, and (b) acrylic-iodine-aluminum thickness distribution measurements.

Figure 6 Estimated thickness distributions of acrylic and iodine. The position $x = 0$ means the center of cylindrical acrylic phantom. Dashed lines are the theoretical thickness distributions.

京都大学 KYOTO UNIVERSITY
A Self-archived copy in
Kyoto University Research Information Repository
https://repository.kulib.kyoto-u.ac.jp
京都大学学術情報リポジトリ KURENAI 紅 Kyoto University Research Information Repository

Figure 7 Two-dimensional maps for (a) acrylic-iodine, and (b) acrylic-aluminum thickness distribution estimation. "Ref." means the reference points *a*~*f* described in Table 1. "Air" means the measured points without acrylic phantom. Solid lines are the scanned results for the acrylic phantom shown in Fig. 5 (b).

Figure 8 Estimated thickness distributions for (a) acrylic (dots) - iodine (squares), and (b) acrylic (dots) - aluminum (triangles), without taking into account the effect of hidden materials.

Figure 9 Schematics for estimating hidden materials (a) aluminum in Fig. 7 (a), and (b) iodine in Fig. 7 (b).

Figure 10 Corrected thickness distributions for acrylic (dots), iodine (squares) and aluminum (triangles). Aluminum thickness 1 mm is normalized to 15 μm thick iodine for easy comparison. Dashed lines are the theoretical thickness distributions.

Figure 11 Calculated number of photons deposited in (a) the first, (b) the second, (c) the third segment detector, and (d) the third segment detector with 300 μm thick Sn filter in front of it as a function of energy. The solid, dashed and broken lines show the photons after passing 16, 18, and 20 cm of acrylic.

Figure 12 Calculated number of photons deposited in (a) the first, (b) the second, (c) the third segment detector, and (d) the third segment detector with 300 μm thick Sn filter in front of it as a function of energy. The solid, dashed and broken lines show the photons after passing 0, 20 and 40 μm thick iodine as well as 20 cm of acrylic.

京都大学 KYOTO UNIVERSITY
A Self-archived copy in
Kyoto University Research Information Repository
https://repository.kulib.kyoto-u.ac.jp
京都大学学術情報リポジトリ KURENAI 紅 Kyoto University Research Information Repository

Table 1

Points	*a*	*b*	*c*	*d*	*e*	*f*
Acrylic (mm)	7	7	7	6	6	6
Iodine (μm)	0	15	30	0	0	0
Aluminum (mm)	0	0	0	0	1	2

京都大学 KYOTO UNIVERSITY
A Self-archived copy in
Kyoto University Research Information Repository
https://repository.kulib.kyoto-u.ac.jp
京都大学学術情報リポジトリ KURENAI 紅 Kyoto University Research Information Repository

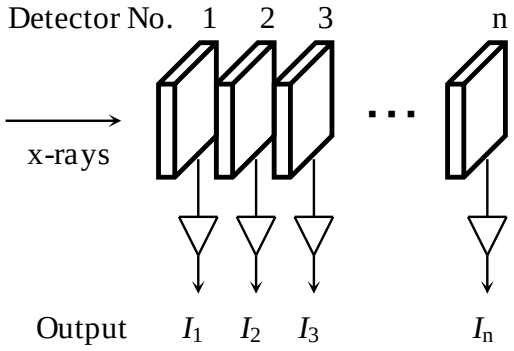

Fig. 1

京都大学 KYOTO UNIVERSITY
A Self-archived copy in
Kyoto University Research Information Repository
https://repository.kulib.kyoto-u.ac.jp
京都大学学術情報リポジトリ KURENAI 紅 Kyoto University Research Information Repository

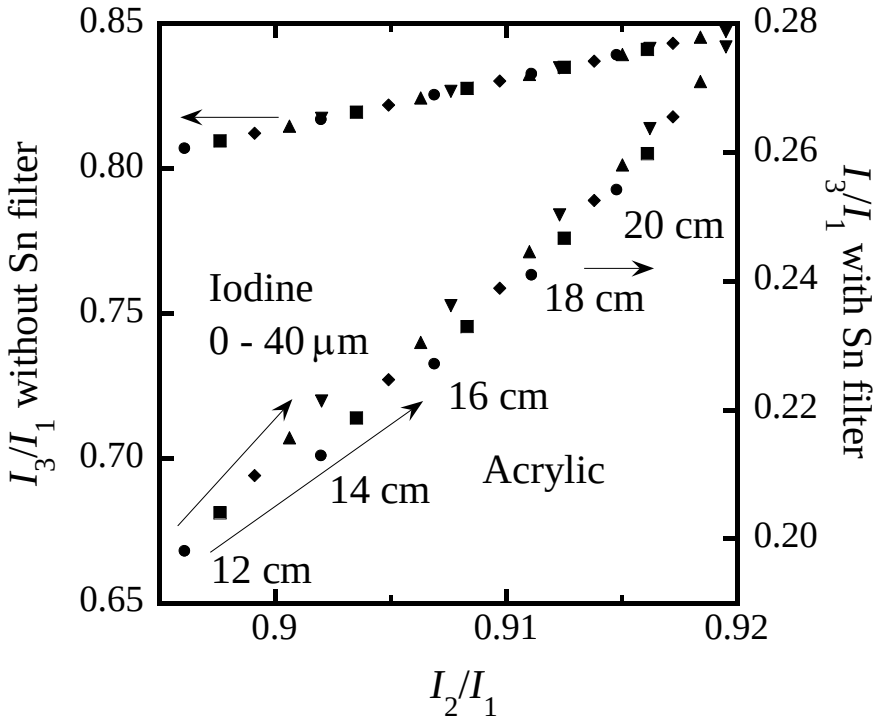

Fig. 2

京都大学 KYOTO UNIVERSITY
A Self-archived copy in
Kyoto University Research Information Repository
https://repository.kulib.kyoto-u.ac.jp
京都大学学術情報リポジトリ KURENAI 紅 Kyoto University Research Information Repository

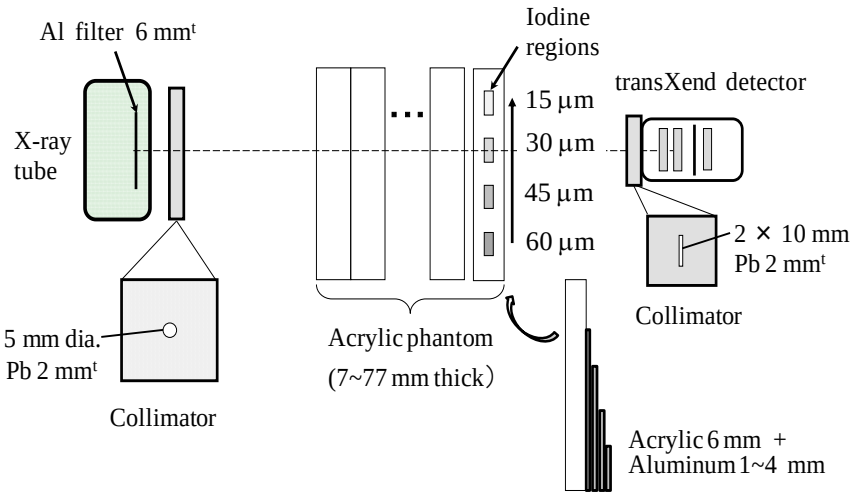

Fig. 3

京都大学 KYOTO UNIVERSITY
A Self-archived copy in
Kyoto University Research Information Repository
https://repository.kulib.kyoto-u.ac.jp
京都大学学術情報リポジトリ KURENAI 紅 Kyoto University Research Information Repository

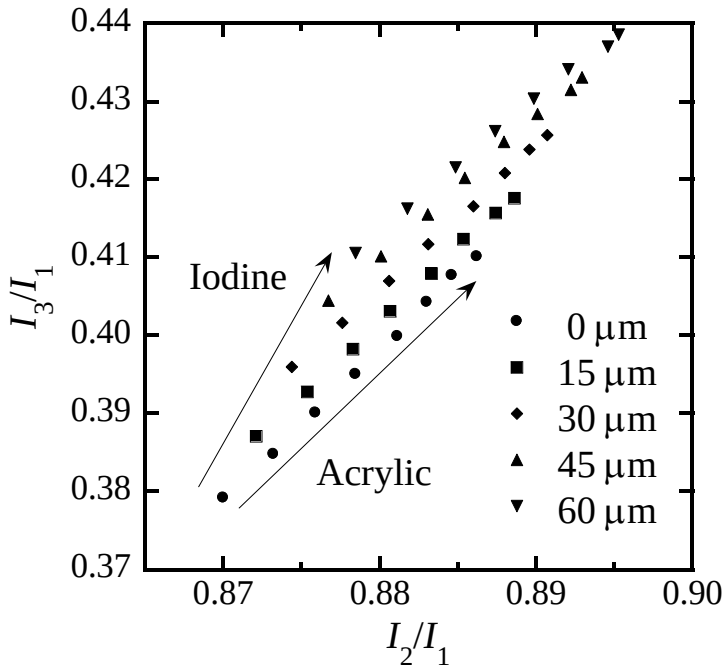

Fig. 4

京都大学 KYOTO UNIVERSITY
A Self-archived copy in
Kyoto University Research Information Repository
https://repository.kulib.kyoto-u.ac.jp
京都大学学術情報リポジトリ KURENAI 紅 Kyoto University Research Information Repository

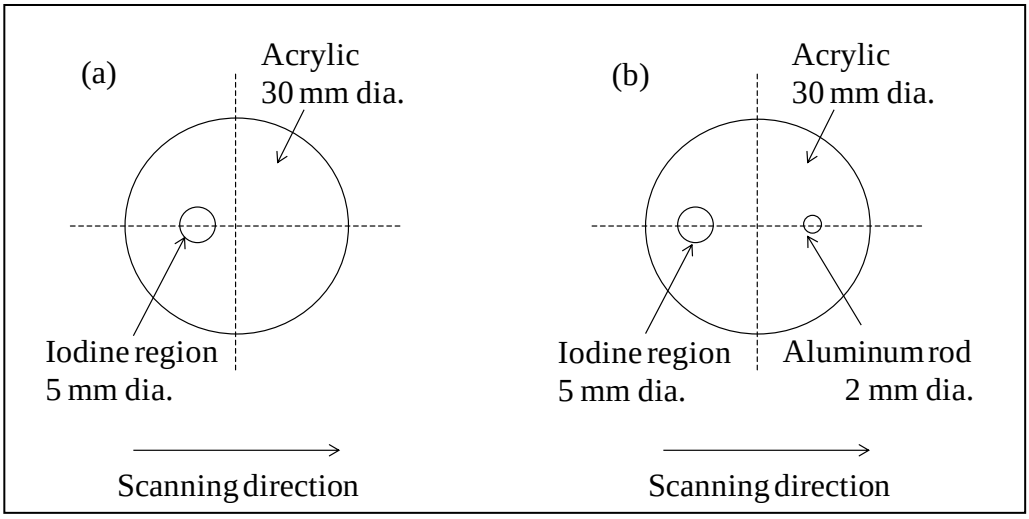

Fig. 5

京都大学 KYOTO UNIVERSITY
A Self-archived copy in
Kyoto University Research Information Repository
https://repository.kulib.kyoto-u.ac.jp
京都大学学術情報リポジトリ KURENAI 紅 Kyoto University Research Information Repository

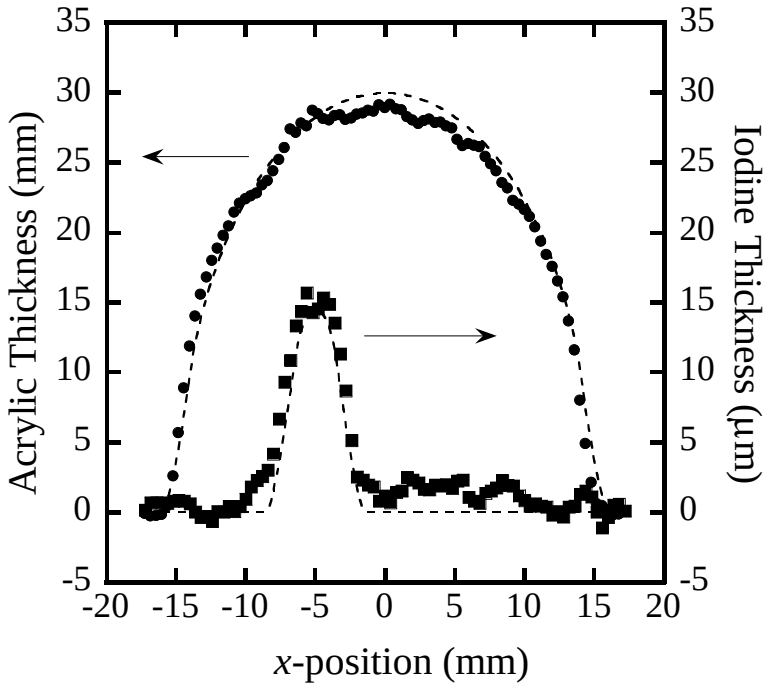

Fig. 6

京都大学 KYOTO UNIVERSITY
A Self-archived copy in
Kyoto University Research Information Repository
https://repository.kulib.kyoto-u.ac.jp
京都大学学術情報リポジトリ KURENAI 紅 Kyoto University Research Information Repository

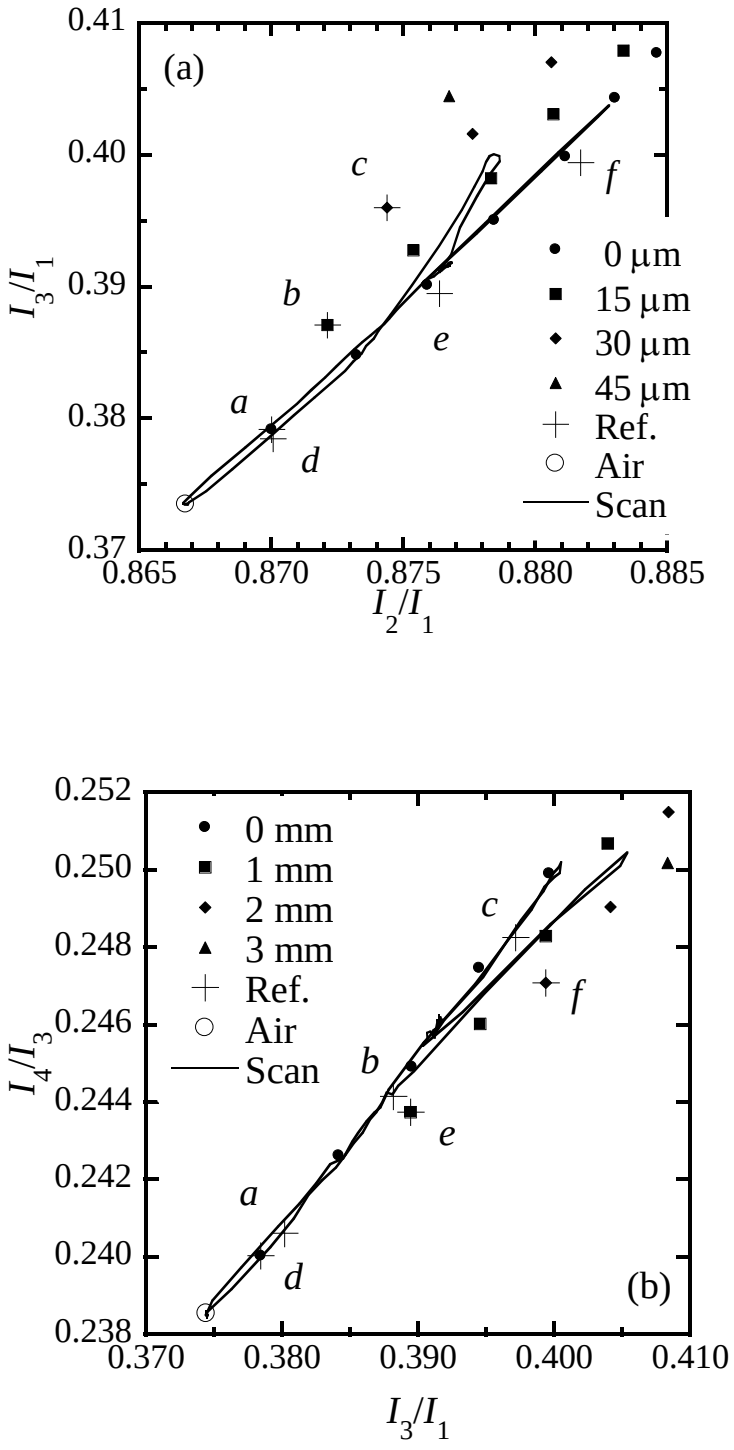

Fig. 7

京都大学 KYOTO UNIVERSITY
A Self-archived copy in
Kyoto University Research Information Repository
https://repository.kulib.kyoto-u.ac.jp
京都大学学術情報リポジトリ KURENAI 紅 Kyoto University Research Information Repository

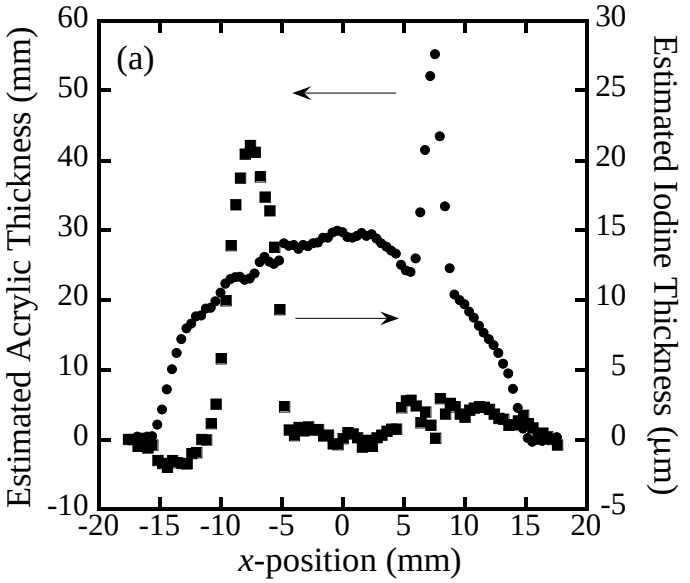

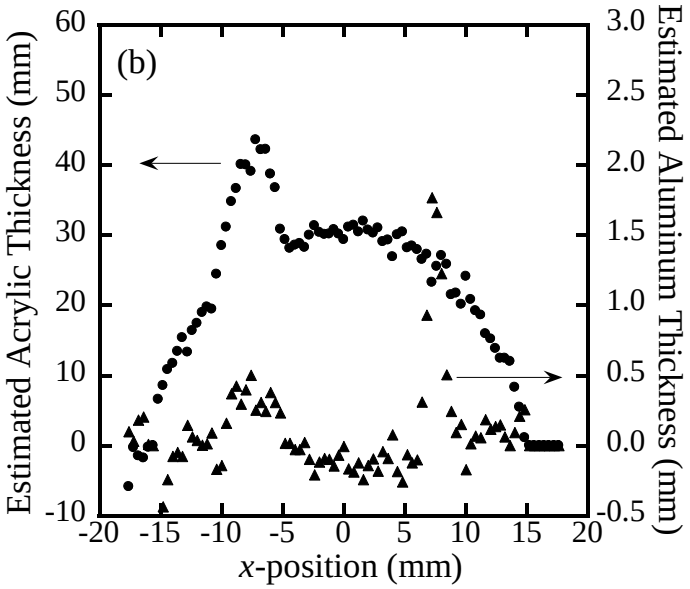

Fig. 8

京都大学 KYOTO UNIVERSITY
A Self-archived copy in
Kyoto University Research Information Repository
https://repository.kulib.kyoto-u.ac.jp
京都大学学術情報リポジトリ KURENAI 紅 Kyoto University Research Information Repository

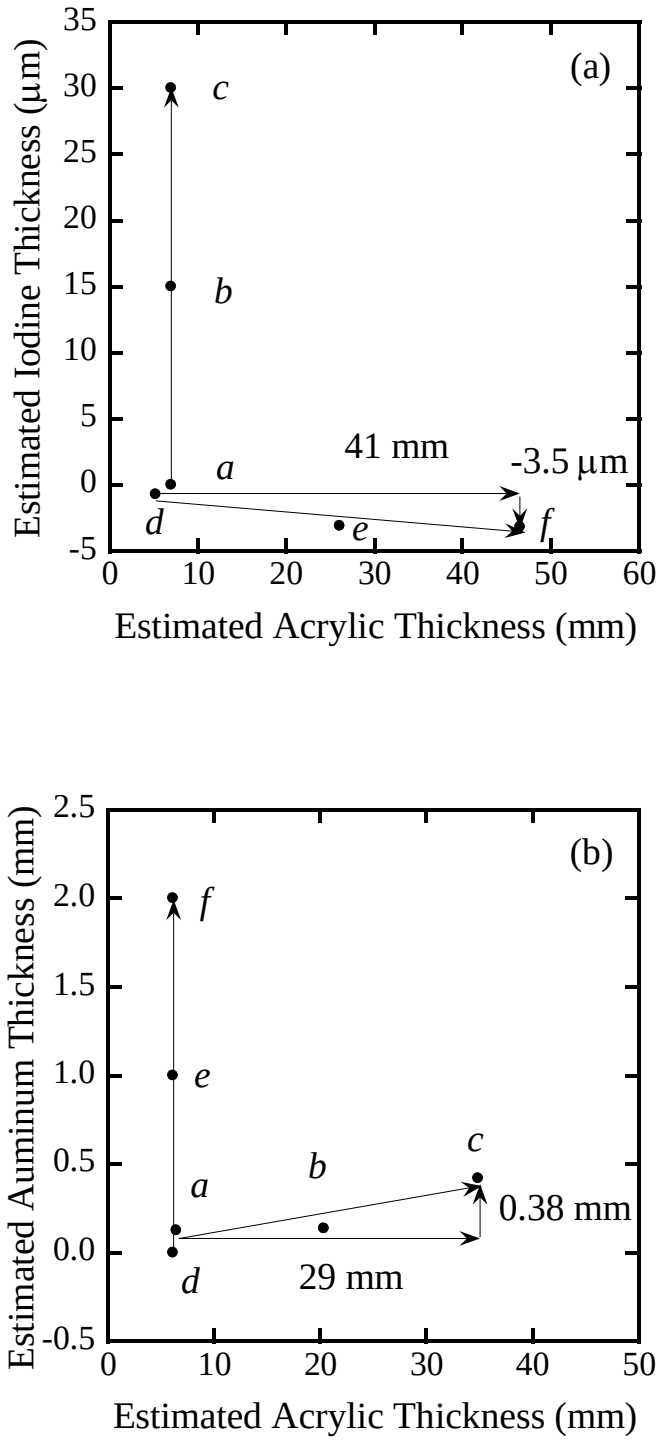

Fig. 9

京都大学 KYOTO UNIVERSITY
A Self-archived copy in
Kyoto University Research Information Repository
https://repository.kulib.kyoto-u.ac.jp
京都大学学術情報リポジトリ KURENAI 紅 Kyoto University Research Information Repository

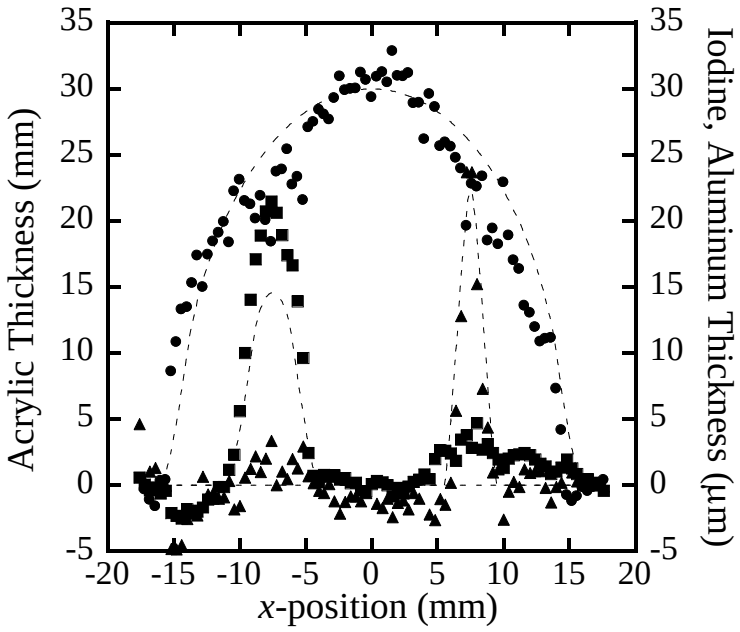

Fig. 10

京都大学 KYOTO UNIVERSITY
A Self-archived copy in
Kyoto University Research Information Repository
https://repository.kulib.kyoto-u.ac.jp
京都大学学術情報リポジトリ KURENAI 紅 Kyoto University Research Information Repository

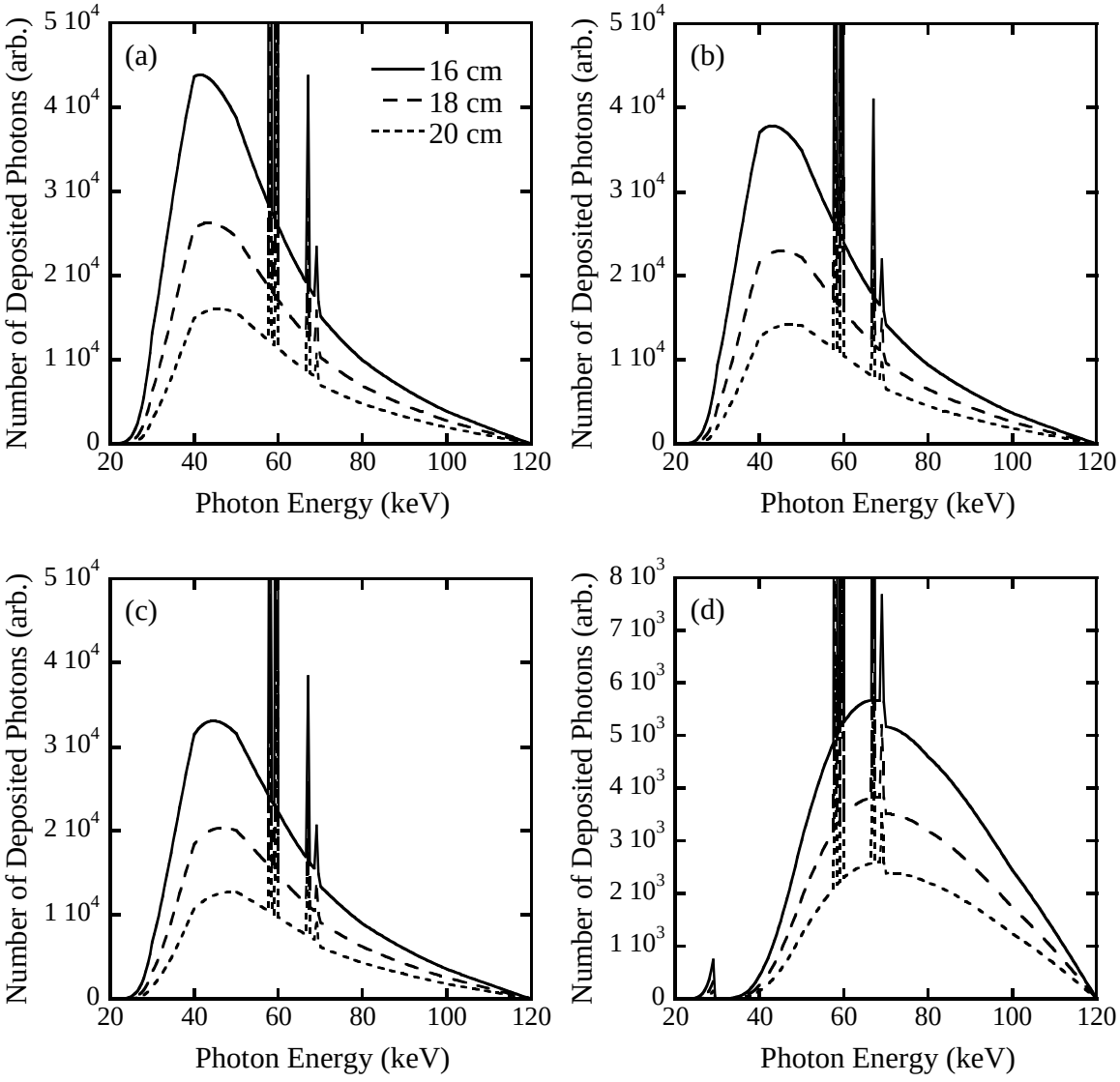

Fig. 11

京都大学 KYOTO UNIVERSITY
A Self-archived copy in
Kyoto University Research Information Repository
https://repository.kulib.kyoto-u.ac.jp
京都大学学術情報リポジトリ KURENAI 紅 Kyoto University Research Information Repository

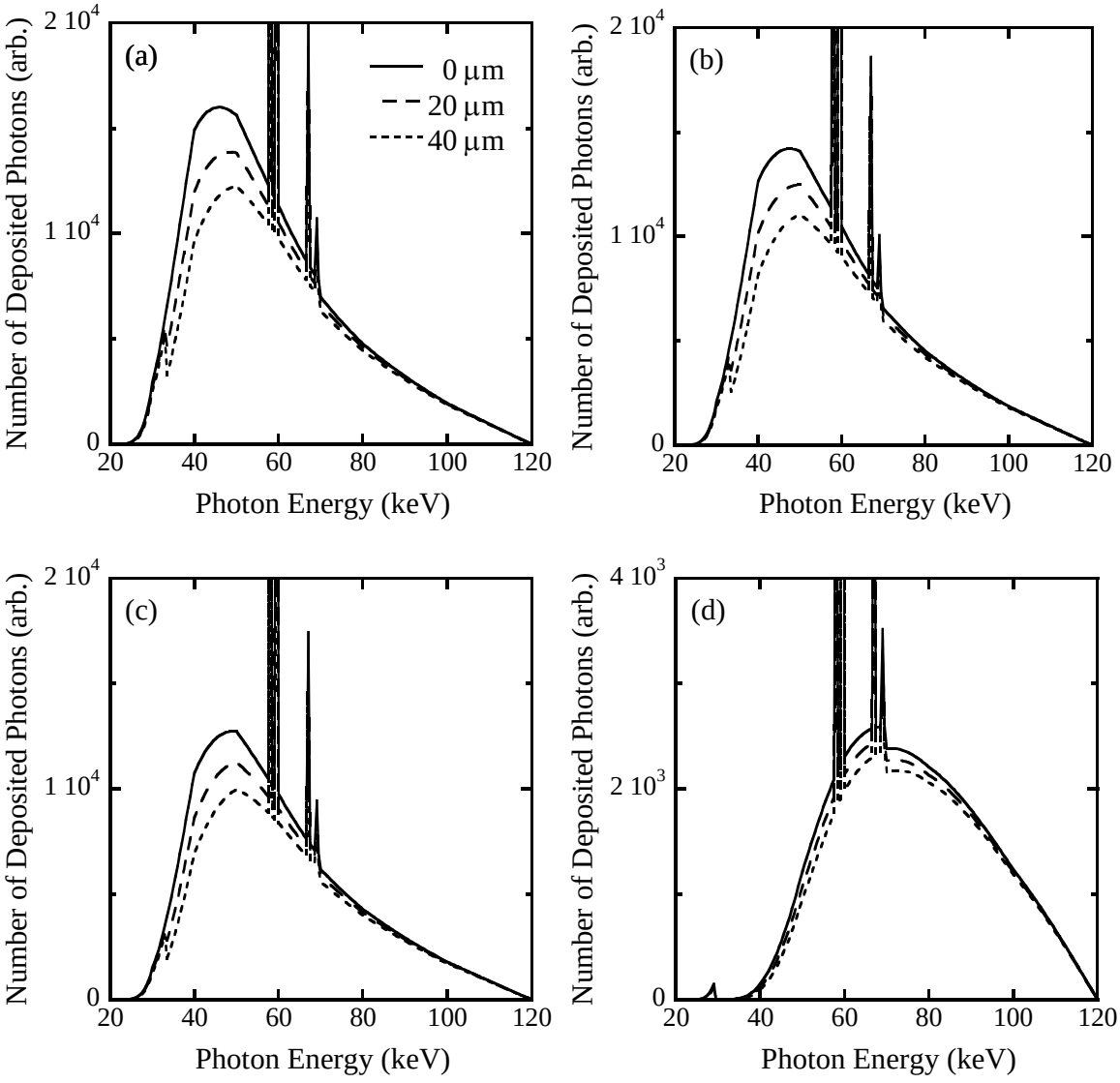

Fig. 12